Biosensors and Bioelectronics 132 (2019) 368–374

Contents lists available at ScienceDirect

Biosensors and Bioelectronics

journal homepage: www.elsevier.com/locate/bios

Fiber optic plasmonic sensors: Providing sensitive biosensor platforms with minimal lab equipment

Nabarun Polley[a,1], Supratim Basak[a,b,1], Roland Hass[a], Claudia Pacholski[a,b,*]

[a] University of Potsdam, Institute of Chemistry, Physical Chemistry – innoFSPEC, Am Mühlenberg 3, 14476 Potsdam, Germany
[b] University of Potsdam, Institute of Chemistry, Karl-Liebknecht-Str. 24-25, 14476 Potsdam, Germany

ARTICLE INFO

Keywords:
Surface plasmon resonance
Optical fiber
Bottom-up fabrication
Biosensor
3D printed flow-cell

ABSTRACT

A simple, convenient, and inexpensive method to fabricate optical fiber based biosensors which utilize periodic hole arrays in gold films for signal transduction is reported. The process of hole array formation mainly relies on self-assembly of hydrogel microgels in combination with chemical gold film deposition and subsequent transfer of the perforated film onto an optical fiber tip. In the fabrication process solely chemical wet lab techniques are used, avoiding cost-intensive instrumentation or clean room facilities. The presented method for preparing fiber optic plasmonic sensors provides high throughput and is perfectly suited for commercialization using batch processing. The transfer of the perforated gold film onto an optical fiber tip does not affect the sensitivity of the biosensor ((420 ± 83) nm/refractive index unit (RIU)), which is comparable to sensitivities of sensor platforms based on periodic hole arrays in gold films prepared by significantly more complex methods. Furthermore, real-time and in-line immunoassay studies with a specially designed 3D printed flow cell are presented exploiting the presented optical fiber based biosensors.

1. Introduction

Biosensing plays an important role in improving the quality of life through reliable and rapid detection of harmful substances. As a result, it applies to many analytical areas ranging from security and defense, point-of-care health care to environmental safety (Cetin et al., 2015; Pumera, 2011). The development of reliable, portable, and affordable biosensors with potential application in a resource-poor environment for the early diagnosis of diseases is indeed a challenge and a need at the same time (Saito et al., 2018). As a possible solution, the use of plasmonic sensors has received considerable attention (Piliarik et al., 2009; Sahoo et al., 2016; Sumner et al., 2000; Wang et al., 2016; Wijaya et al., 2011). In this case, surface plasmon resonance (SPR), i.e., a collective oscillation of free electrons at the metal/dielectric interfaces driven by electromagnetic waves, has been used for signal transduction in optical sensors. Two different kinds of SPR can be investigated for this purpose: localized surface plasmon resonance (LSPR, Mayer and Hafner, 2011) and propagating surface plasmon resonance (PSPR, Yonzon et al., 2004). The first occurs in nanoparticles with a diameter much lower than the wavelength of light used for detection, can be directly excited by light, and is sensitive to refractive index changes taking place maximal 10–20 nm above their surface. The latter are composed of gold films and cannot be directly excited by light, but require either a prism or a grating in the gold film for this purpose. The exceptional interest in PSPR sensors is based on their high sensitivity, which can be traced back to a larger examination volume resulting from the penetration depth of PSPR into the surrounding medium. Here, refractive index changes up to several 100 nm above the gold film can be detected. However, the often bulky optical instrumentation of PSPR sensors (Jian et al., 2014) limits their actual applicability, especially in remote areas or in point-of-care devices.

This challenge can be addressed by combining PSPR sensor platforms with optical fibers. In general, the tremendous advantages of equipping optical fibers with plasmonic structures have already been demonstrated - especially for LSPR signal transduction (Jian et al., 2014; Riccardi et al., 2015; Klantsataya et al., 2017; Liu et al., 2017). Very compact optical fiber tip-based devices can be obtained in this way, which are cheap, flexible, robust, lightweight, highly sensitive, and available in various sizes. Here, patterning the facets of optical fibers with plasmonic nanostructures opens the door for several application areas, e.g., label-free biological analyses for extremely small volume of samples (Cetin et al., 2015; Lin et al., 2011) or inline real-time biosensing (Jia and Yang, 2014).

However, because of the inherent small dimensions of optical fibers,

* Corresponding author.
E-mail address: cpachols@uni-potsdam.de (C. Pacholski).
[1] Contributed equally.

https://doi.org/10.1016/j.bios.2019.03.020
Received 23 November 2018; Received in revised form 8 March 2019; Accepted 11 March 2019
Available online 12 March 2019
0956-5663/

it is very difficult to handle them in established processes for nano/microstructuring on the fiber core surface or fiber tip. Notably, spin coating of resist on optical fibers, or mounting optical fibers in electron beam writers/photolithographic chambers is cumbersome. Mainly three types of methodologies have been adopted for circumventing these challenges:

i) Direct patterning of the optical fiber tip by conventional hard lithography, e.g., electron beam lithography (EBL) (Consales et al., 2012) or focused ion beam (FAB) milling (Dhawan et al., 2008). However, main drawbacks of these methods are that they require sophisticated apparatus and cleanroom facilities, which are beyond the reach of many laboratories. Furthermore, the fabrication process also suffers from low throughput and hence low yield of nanostructured optical fibers.
ii) Preparation of nanostructures by hard lithography and their subsequent transfer to optical fiber tips. This approach reduces complicacy regarding fiber alignment and handling of long optical fibers in the electron beam/photolithography chamber, but introduces an additional transfer step. Utilization of adhesives for the attachment of the prefabricated nanostructure to the optical fiber is common but undesirable due to its poor reproducibility (Najiminaini et al., 2011; Siegfried et al., 2013). The transfer can be achieved by exploiting thiol-ene films (Smythe et al., 2009) or by nanoskiving (Lipomi et al., 2011). Hexagonal, square (Jia and Yang, 2014), and quasi periodic (Jia et al., 2016) gold nano hole arrays were generated on fiber tips with this technique.
iii) Fabrication of nanostructures by self-assembly utilizing hard spheres in combination with plasma etching (PE) and subsequent transfer on fiber tips. Unlike the above two methods this process only involves PE regarding costly equipment. Therefore, a high throughput and high yield can be reached. The procedure is simple but not trivial for patterning optical fiber tips. To the best of our knowledge there is only one article which utilizes this fabrication strategy (Pisco et al., 2017). In this case, the obtained optical fiber probes with periodic hole arrays in a thin (~40 nm height above the substrate surface) gold film have not yet been investigated for sensing purposes.

In general, it is quite surprising that there are only a few studies on the detection of biomolecules using plasmonic optical fiber sensors exploiting PSPR for signal transduction (Dhawan and Muth, 2008; Lan et al., 2014). Commercial PSPR sensor devices have mainly been developed for monitoring biomolecular binding events in real-time and their success story is based on their relevance in several research areas including proteomics and drug discovery (Florinskaya et al., 2018). Until now, miniaturization of these PSPR sensors has mainly been obtained by combination with microfluidic systems. The potential of PSPR sensor platforms integrated with optical fibers has barely been tapped and the commercialization of this type of fiber optic plasmonic sensors has not yet been seriously tackled.

In order to address all the above-mentioned challenges, a fast, low-cost chemical approach to prepare periodic hole arrays in gold films on optical fiber tips was developed (Fig. 1). For this purpose, self-assembly of hydrogel microspheres accompanied with electroless platting was used as demonstrated elsewhere (Quint and Pacholski, 2009). Subsequently, the periodic hole array in a gold film was lifted off from the glass slide support by reaction with NaOH and transferred to the optical fiber tip. Hereby, the periodic hole arrays in gold films was bound to the optical fiber tip surface via a linker, namely 3-aminopropyltriethoxysilane, which was deposited on the optical fiber tip surface prior to the transfer process. As the proposed method is capable of fabricating periodic hole arrays in gold films on large areas, it is possible to pattern many optical fiber tips at a time and hence a mass production of sensors can be easily achieved. A rough estimation of the number of fiber plasmonic sensors prepared using a single periodic hole array, which was previously fabricated on a flat glass substrate, can be found in the Supporting information.

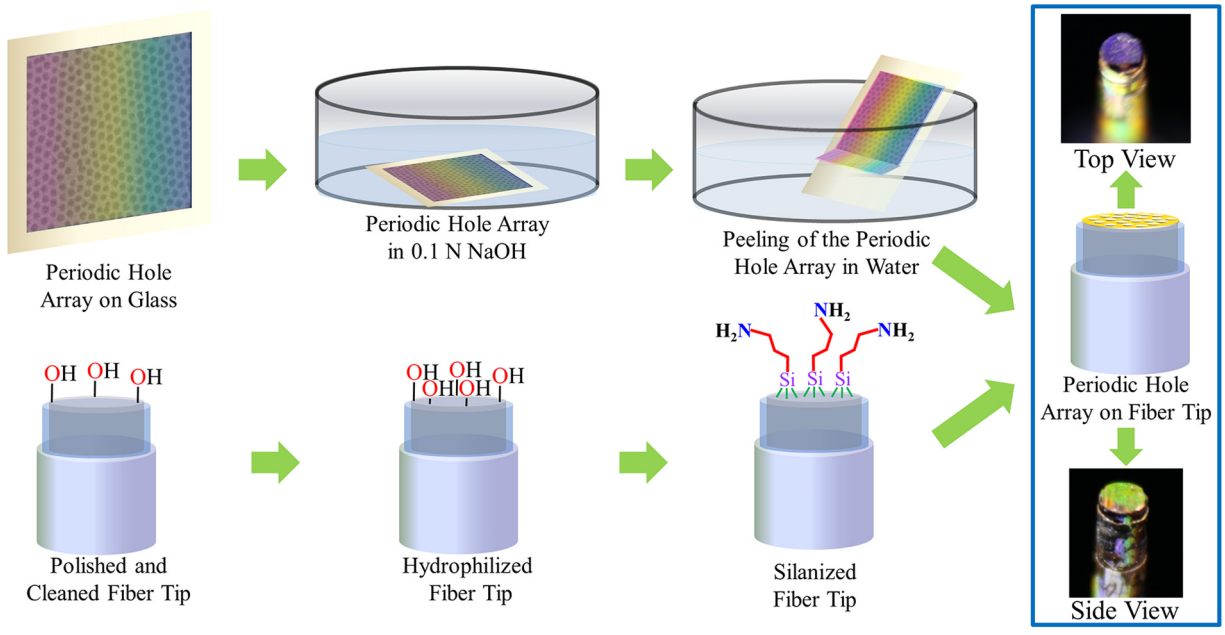

Fig. 1. Process used to prepare fiber optic plasmonic sensors. A periodic hole array in a gold film is fabricated on a flat glass substrate using solely chemical methods. Subsequently, this hole array is lifted off from the substrate surface by immersing it in basic solution. The hole array film detaches from the substrate surface and starts floating on water surface. The periodic hole array in a gold film can be picked up with an appropriately functionalized optical fiber tip. Photographs of the resulting fiber optic plasmonic sensors are shown on the right hand side.

Moreover, biosensing experiments using protein A as capture probe and rabbit or goat immunoglobulins (IgGs) as target analytes were carried out and equilibrium binding constants were determined. Protein A is often used for immobilizing specific antibodies to immuno-sensing devices as it ensures proper orientation of the bound antibody (Boujday et al., 2008).

2. Materials and methods

2.1. Materials

Tetrachloroauric acid ($HAuCl_4{\cdot}3H_2O$), hydroxylamine hydrochloride ($HONH_2{\cdot}HCl$), ascorbic acid ($C_6H_8O_6$), glutaraldehyde ($C_5H_8O_2$), cystamine, (3-aminopropyl)triethoxysilane (APTS), IgG from rabbit and goat were obtained from Sigma-Aldrich Chemie GmbH, Germany. All other chemicals including sodium hydroxide (NaOH), sodium chloride (NaCl), acetic acid, and isopropanol were supplied by Carl Roth GmbH + Co. KG, Germany. Hellmanex-III was purchased from Hellma GmbH & Co. KG, Germany. For all the experiments, ultrapure water (impedance 18 MΩ) from a commercial Milli-Q® Integral system (Merck Chemicals GmbH, Germany) was used. Preparation of sensors was carried out on glass slides with dimension 24 mm × 24 mm × 0.17 mm, which were purchased from Carl Roth GmbH + Co. KG, Germany. Optical fibers (JTFLH6006301040) with a core diameter of 600 μm were received from Laser Components GmbH (Olching, Germany). An optical fiber bundle (16–1, optical fiber core diameter: 100 μm) from Loptek GmbH & Co. KG (Berlin, Germany) coupled to a HL-2000 light source from Ocean Optics (Florida, USA) in one channel and to a QE65 Pro spectrometer (Ocean Optics) at the other channel was used to guide and collect light to and from the sensor, respectively. Four computer controlled dosing pumps SP-50 from Mettler Toledo (Gießen, Germany) were employed to provide alternating controlled flow of chemicals through the self-developed, 3D printed flow cell from Shapeways (New York, USA) incorporating the fiber optical biosensor. For characterization of the fabricated sensors a Quanta 250 electron microscope from FEI Deutschland GmbH (Frankfurt am Main, Germany) was used. Atomic force micrographs were obtained using a WITec alpha300AR device from WITec Wissenschaftliche Instrumente und Technologie GmbH (Ulm, Germany). In order to measure the refractive index of different media during the study, a refractometer ATR-L from -SCHMIDT + HAENSCH GmbH & Co (Berlin, Germany) was used.

2.2. Methods

2.2.1. Fabrication of periodic hole arrays in gold films

Periodic hole arrays in gold films were first prepared on glass cover slips according to Quint and Pacholski (Quint and Pacholski, 2009). Briefly, poly-N-isopropylacrylamide (poly(NIPAM)) microgels were synthesized and washed several times with ultra pure water to remove any impurities by centrifugation (with a temperature above 32 °C) and decantation. Then, the microgel dispersion was diluted with ultra pure water (poly(NIPAM):water, 1:49, v-v). Glass cover slips were immersed in a solution of Hellmanex (2% in water, v:v) overnight prior to use in order to make the surface hydrophilic. Then they were thoroughly rinsed with ultra pure water, blown dry in a stream of nitrogen, and placed on a custom-made, low-cost spin-coater. 40 μL of the diluted poly(NIPAM) dispersion was added on the glass cover slip, followed by addition of 2 × 40 μL ethanol. After covering the whole glass surface by the mixture, another 40 μL of ethanol was added. The spin coating process was carried out at low speed (Quint and Pacholski, 2011).

All parts of the film preparation were performed at room temperature. At the end of the spin coating process, an iridescent color on the glass cover slips could be noticed resulting from the hexagonally ordered poly(NIPAM) colloidal array. In the next step, the spin coated glass cover slips were silanized by keeping them in a tightly sealed glass container (Carl Roth GmbH + Co. KG, Germany, radius 90 mm, height 73 mm) along with 150 μL of diluted APTES (150 μL of APTES in 10 mL of isopropanol). The glass containers were kept at 100 °C in a hot air oven (Heraeus, Hanau, Germany) for 1.5 h and then cooled to room temperature. Finally, the silanized poly(NIPAM) coated slides were taken out from the glass containers and thoroughly rinsed with ultra pure water and again kept in the oven at 100 °C for 1 h.

Gold nanoparticles, prepared according to Turkevich et al. (1951), were deposited on the glass surface after silanization. The preheated gold nanoparticle dispersion (500 μL at 40 °C) was placed on top of each coated slide, which was afterwards incubated at 40 °C for 1 h in a closed plastic container. Later the slides were rinsed thoroughly with ultra pure water and allowed to dry in ambient atmosphere. The deposition of Au nanoparticles could easily be observed by a pinkish appearance of the glass cover slides. For the formation of the gold film, an electroless plating process was performed (Guan et al., 2005). First, an electroless plating aqueous solution was prepared by adding 150 μL of 40.30 mM hydroxylamine hydrochloride solution to 10 mL of a 12.70 mM $HAuCl_4{\cdot}3H_2O$ solution. Then 2 mL of the solution was kept in a plastic container (Plano GmbH, Germany, 30 mm × 30 mm × 4.8 mm) and the gold nanoparticle coated films were kept upside down on the surface of the reaction solution for 1.5 h to form a thin smooth Au film. In the last fabrication step, the poly(NIPAM) mask was removed by flame annealing of the samples in a 80% butane/20% propane flame.

2.2.2. Transferring the periodic hole array in a gold film on the fiber tip

The transfer process of the periodic hole array in a gold film from the glass slide on to the fiber tip was achieved in two steps (Fig. 1): Glass cover slides with periodic hole arrays in gold films were incubated in a 0.1 N aqueous solution of NaOH overnight in order to break the covalent bond between the gold film and the glass surface in accordance with Weiler et al. (Weiler et al., 2014). Then, a line was carefully scratched with a tweezer tip into the gold film and upon immersing the glass slides in ultra pure water the gold film detached from the glass surface. The periodic hole array in a gold film floating on the water surface was then transferred to the optical fiber tip. For this purpose, fiber tips were cleaned by bath sonication in commercial detergent solution for 30 min to remove any oil and residual material from the fiber surface. Afterwards, the fiber tips were sonicated in a water-ethanol mixture for another 30 min. The cleaned fiber tips were then immersed in a solution of Hellmanex (2 vol% in water) and kept overnight followed by silanization of the fiber tips with APTES as described before. Finally, the periodic hole arrays in gold films were lifted up from the water surface utilizing the optical fiber tips. For this purpose the optical fiber was brought into contact with a periodic hole array in a gold film floating at the air/liquid interface. The periodic hole array in a gold film was bound to the optical fiber surface via the present amine groups. Afterwards, the optical fiber was pulled away from the air/liquid interface under an angle. In this moment the periodic hole array in a gold film was teared off the unbound periodic hole array in a gold film still floating at the air/liquid interface. Then the optical fiber plasmonic sensor was dried in a hot air oven at 80 °C for 1 h. During the drying process the periodic hole array in a gold film was tightly bound to the fiber surface via the amine-groups of APTES. On the right hand side of Fig. 1 the “side view” and “top view” of such a fabricated sensor are shown. It is worth mentioning that the optical appearance of the periodic hole array in a gold film depends on the angle of view as observed in the inset figures (right, top and bottom). This provides a very simple test that can be performed with the naked eye to see the successful transfer of the plasmonic structure to the fiber tip.

2.2.3. Biosensor fabrication

In order to demonstrate the label-free sensing capabilities of optical fibers decorated with periodic hole arrays in gold films, the fibers were equipped with Protein A according to a method described by Boujday et al. (2008). For this purpose, the fiber optic plasmonic sensors were

immersed in 1 mL of a 10 mM aqueous solution of cystamine for 12 h, rinsed thoroughly with ultra pure water, and dried in a stream of nitrogen. Then, the sensors were dipped in 1 mL of a 0.1 M solution of glutaraldehyde in ethanol for another 12 h. Finally, they were extensively rinsed with ethanol and immersed in 1 mL of a 0.1 mg mL^{-1} solution of Protein A in phosphate buffered saline solution (PBS). After 3 h, the sensors were washed several times with PBS and utilized for label-free biosensing experiments.

2.2.4. Determination of reflectance minima

Reflectance spectra were recorded every 2 s, 5 s, or 10 s (depending on the time frame of the experiment) with an integration time of 30 ms and 10 averaged scans. For better tracking of the plasmonic minima during the experiment, a Matlab-based program was used. Briefly, the position of the reflectance minimum in each recorded spectrum was determined by a fitting routine. The routine at first determined the absolute minimum. This minimum was taken as starting point. Then, 256 data points of the experimental spectra were chosen, which surrounded this minimum, and fitted these points with the polyfit Matlab function with a degree of n = 5 ($f(x) = p_1x^5 + p_2x^4 + p_3x^3 + p_4x^2 + p_5x + p_6$). Finding overall minima over a region rather than finding out a single minimum from the raw data is more consistent in order to overcome noise. Apart from that, the fitting routine is necessary for the statistical treatment of handling large amount of data.

3. Results and discussion

3.1. Characterization of the fiber optic plasmonic sensors

In order to characterize fabricated periodic hole array in a gold film, which have been transferred to a fiber tip, scanning electron microscopic (SEM) studies were carried out. Fig. 2(a) shows a representative SEM image of a periodic hole array in a gold film successfully deposited on a fiber tip.

A magnified view of the periodic hole array in a gold film on the fiber tip is displayed in the inset of Fig. 2(a). The good degree of order in the prepared periodic hole arrays in gold films can be easily noticed. By calculating the radial distribution function (Quint and Pacholski, 2014; Rengarajan et al., 2005; Ullrich et al., 2013) of the holes using the presented SEM image (Fig. S1) regular domains with a diameter of 7–10 lattice constants can be estimated. The lattice constant is found to be 411 nm with a standard deviation of 67 nm. The diameter of the holes and the open area fraction of the periodic hole arrays in gold films can be obtained using already established plugins in the software ImageJ. The periodic hole array in a gold film shown in Fig. 2(a) had an open area fraction of 36.5% and the diameter of the holes was 251 nm with a standard deviation of 18 nm. Furthermore, the gold film thickness of the periodic hole array in a gold film before transferring to the optical fiber tip was determined by atomic force microscopy to be 61 nm with a standard deviation of 9 nm (data not presented). All these parameters have a direct influence on the optical properties of the presented fiber optic plasmonic sensor. In Fig. 2(b) transmission and reflectance spectra of a prepared periodic hole array in a gold film deposited on a glass substrate before transfer to the tip of an optical fiber are displayed. These spectra are presented in order to unravel the origin of the SPR peaks in the optical spectra. The most pronounced transmission maximum located at ~780 nm can be assigned to the (1,0) gold/glass resonance of the periodic hole array using the following equation (Thio et al., 1999):

$$\lambda_{max} = \frac{a_0}{\sqrt{\frac{4}{3}(i^2 + j^2 + ij)}} \sqrt{\frac{\varepsilon_d \varepsilon_m}{\varepsilon_d + \varepsilon_m}} \quad (1)$$

where λ_{max} is the resonance wavelength, a_0 is the lattice constant of the array, and i as well as j are integer numbers reflecting the Bragg resonance order. ε_m and ε_d are the dielectric constants of the metal and the dielectric medium, respectively, representing the dependence of the position of the transmission maximum on the refractive index n of the surrounding medium (including the sample solution), because $n = (\varepsilon_{real})^{\frac{1}{2}}$. The transmission maximum is based on the excitation of PSPR as well as LSPR. The phenomenon is also referred to as extraordinary transmission of light (EOT). The EOT peak from the transmission spectrum appears as a minimum in the reflectance spectrum in air. Furthermore, a second transmission maximum located at 560 nm can be noticed which can be assigned to the (1,0) gold/air resonance of the periodic hole array. Fig. 2(c) shows reflectance spectra of the periodic hole array in a gold film deposited on the fiber tip in comparison to an unstructured gold film with the same thickness. Both spectra were recorded in air. The presence of a reflectance minimum at around

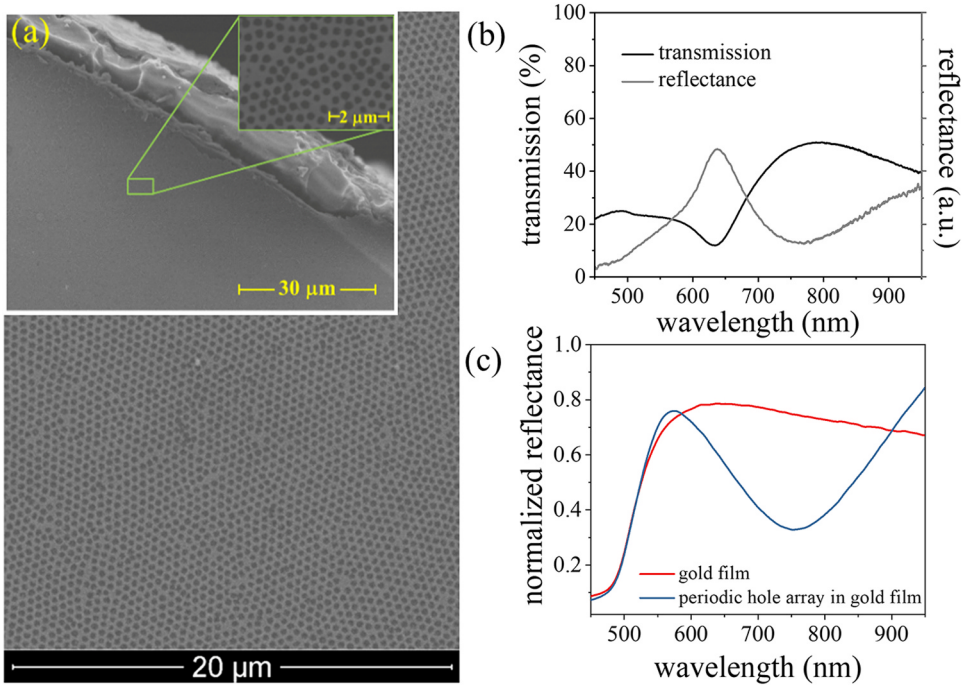

Fig. 2. Characterization of fabricated fiber optic plasmonic sensors. (a) Scanning electron microscope images of a periodic hole array in a gold film on a fiber tip taken at low and high magnification (insets). (b) Transmission and reflectance spectra of a periodic hole array in a gold film on a glass substrate before transferring to a fiber tip. (c) Comparative normalized reflectance spectra of a gold film with and without a periodic hole array deposited on the end facet of an optical fiber.

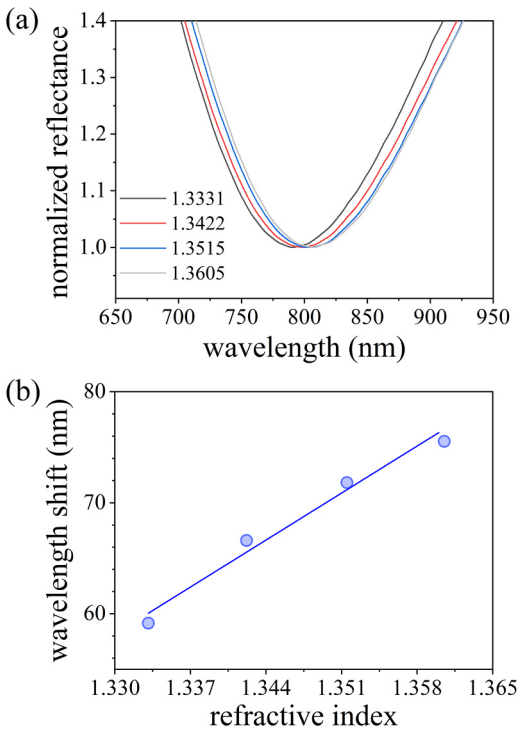

Fig. 3. (a) Red shift of the plasmonic band with increasing refractive index of glucose solutions from 1.3331 to 1.3605 (see text for more details). (b) Determination of the sensitivity of the plasmonic optical fiber sensor using the position of the reflectance minimum in (a).

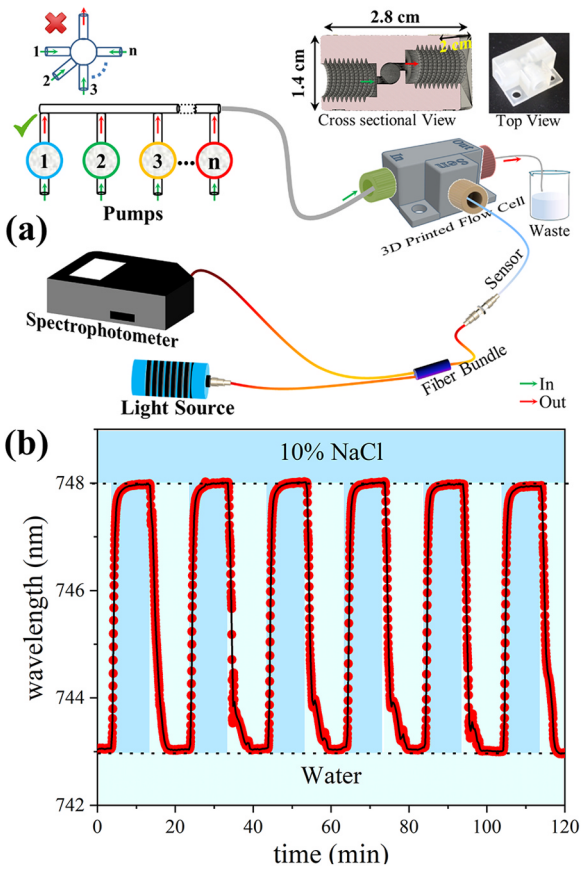

Fig. 4. (a) Experimental setup for continuous detection of refractive index changes using a custom-made 3D printed flow cell. (b) Monitoring wavelength change using the fabricated fiber optic plasmonic sensor in combination with the experimental setup presented in a). Water with n_{water} = 1.329322 and 10% NaCl solution with $n_{10\%\ NaCl}$ = 1.345534 (both at a wavelength of 742 nm and at 20 °C) were flown over the sensor surface in 6 consecutive cycles.

450 nm in both fibers is attributed to the gold film itself (McMahon et al., 2007) and the instrumental response. The second reflectance minimum located at ~ 760 nm is resulting from the periodic hole array in a gold film and is assigned to the EOT peak.

3.2. Sensitivity of the fiber optic plasmonic sensor

The sensor performance was investigated by measuring reflectance spectra upon immersion of the sensor (fiber tip) in aqueous glucose solutions having different refractive indices. The red shift of the position of the reflectance minimum at ~780 nm on the wavelength scale with increasing refractive index (*n*) is evident from Fig. 3(a).

In order to determine the sensitivity of the fiber optic plasmonic sensor, the shift of wavelength for minimal reflectance vs. the refractive index of the solution determined at 742 nm (Fig. 3(b)) was plotted. A linear relation between wavelength shift and refractive index can easily be noticed (r = 0.9885). The slope of this linear relation is defined as sensitivity and was determined to be 593 nm/RIU with a standard deviation of 64 nm/RIU in this case (Table S1, sensor B2_S1). In Table S1 determined sensitivities of six separate sensors are presented. These six sensors were prepared using three separate periodic hole arrays in gold films pre-formed on glass substrates (= three batches) which were subsequently transferred to an optical fiber tip. Sensitivities were determined using the fiber optic plasmonic sensors and an average sensitivity of (420 ± 83) nm/RIU was obtained. Considering the fabrication strategy for these sensors, which is based on self-assembly of hydrogel microspheres and chemical gold deposition, the variation of their sensitivities is acceptable, but may need further attention in future work. However, the sensitivity of the presented sensor is comparable to similar sensors fabricated by using more sophisticated methods such as ion beam milling (Dhawan et al., 2008: 530 nm/RIU) or electron beam lithography in combination with a transfer process (Jia and Yang, 2014: ~330 up to ~500 nm/RIU, depending on the position of the reflectance minimum on the wavelength scale). It is worth mentioning that the degree of order of the hole array and other factors, such as hole morphology (Menezes et al., 2012) or the geometrical lay-out of the holes (Ekşioğlu et al., 2016), have an influence on the sensitivity of these plasmonic sensors.

3.3. Continuous detection of refractive index changes in a flow cell setup

To establish the application of the fiber optic plasmonic sensor as a potential label-free and real-time biosensor, a flow cell setup was developed. For this purpose, a simple design and manufacturing strategy, namely additive manufacturing, was chosen in order to provide easy access to a complete sensor setup. The experimental setup for continuous detection of refractive index changes is represented in Fig. 4(a) and Fig. S2. A special purpose 3 channel flow cell with physical dimension of 2.8 cm × 2.0 cm × 1.4 cm was designed and 3D printed from a commercial company. For 3D printing, Material Jetting (MJ) of UV curable acrylic plastic material was chosen due to its high-resolution printability (layer thickness 16 µm). The two arms of the "T" shaped flow cell are assigned as 'input' (green arrow, Fig. 4(a)) and 'output' (red arrow, Fig. 4(a)). The middle channel is intended for optical signal transduction and therefore connected to an optical fiber for transmitting and collecting light to and from the sensor, respectively. Horizontal off-axis placement of 'input' and 'output' channels around a common spherical sensing region with a 'sensing' channel in the middle results in a bubble-free measurement (Inset Fig. 4(a)).

For monitoring biomolecular interactions using the developed sensor, different solutions have to be passed over the sensor surface. A conventional single pump (Thio et al., 1999; McMahon et al., 2007)

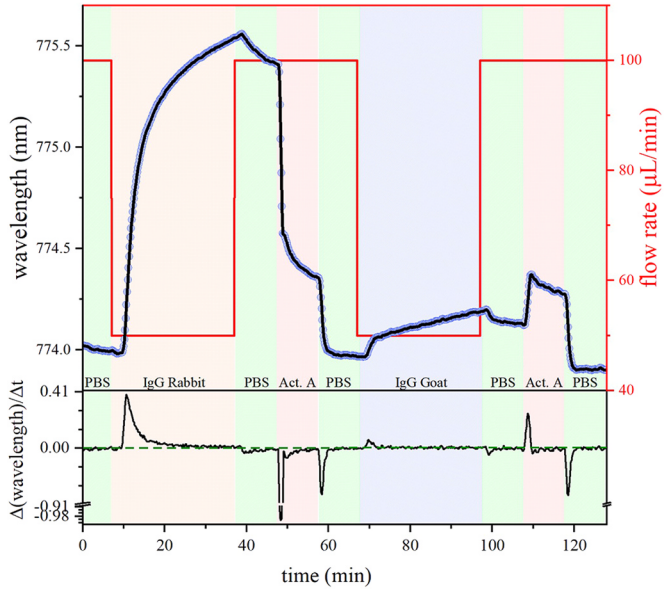

Fig. 5. Optical response of the fiber optic plasmonic sensor modified with Protein A to the addition of IgG from rabbit (40 μg mL^{-1}) and IgG from goat (40 μg mL^{-1}). At the bottom the numerical first derivative of the optical response is shown, demonstrating the achievement of equilibrium binding conditions.

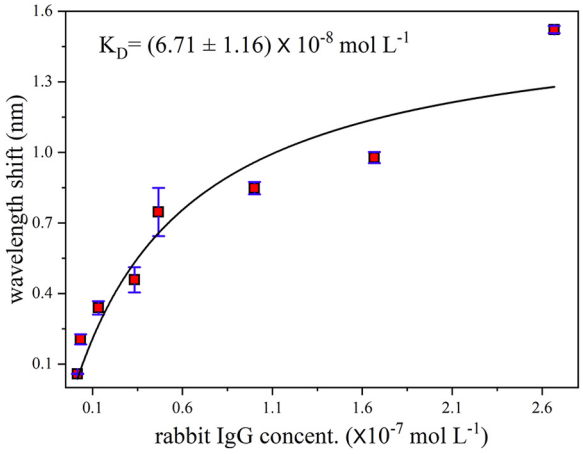

Fig. 6. Wavelength shift as function of concentration of IgG from rabbit at equilibrium of the fiber optic plasmonic sensor. The equilibrium dissociation constant for rabbit IgG/Protein A was determined through a fit of the binding curve to a Langmuir isotherm (K_D = (6.71 ± 1.16) × 10^{-8} mol L^{-1}).

could be employed for this purpose. However, this strategy has several shortcomings like more bubble problems (introduced mostly during change of the sample), high chance of contamination (due to usage of the single syringes over the entire experiment), and full time involvement during the experimental period. Using multiple pumps in serial implementation could be the potential solution to this problem. Here, four pumps connected in a special geometry to avoid possible interaction of different solutions with each other during the experiment were utilized (presented in Fig. 4(a)).

The flow rate of the solutions was chosen to be 100 μL min^{-1} - unless otherwise stated. The functionality of the flow cell setup was tested by passing different solutions alternately over the sensor surface (B3_S1 Table_S1) - namely 10% NaCl aqueous solution ($n_{10\%\ NaCl}$ = 1.345534 at 742 nm and 20 °C) and water (n_{water} = 1.329322 at 742 nm and 20 °C). Multiple cycles demonstrate the reproducibility and reliability of the measurement (Fig. 4(b)).

3.4. Inline label-free bio sensing

To demonstrate the potential as label-free and real-time biosensor, an immunoassay study was performed between Protein A and IgG from rabbit as well as IgG from goat as control. The different solutions were transported through the flow cell by using different pumps: Pump 1: phosphate buffered saline (PBS), Pump 2: IgG Rabbit in PBS, Pump 3: IgG Goat in PBS, and Pump 4: acetic acid (0.1 M). Tubings and flow cell were cleaned with PBS thoroughly before the experiment. A single biosensing experiment is shown in Fig. 5.

First, PBS was passed over the sensor in order to establish a constant baseline (0–7 min). During this time the position of the plasmonic band is located around 774 nm. Then, a 40 μg mL^{-1} IgG from rabbit solution in PBS with a flow speed of 50 μL min^{-1} was introduced. A red shift in the position of reflectance minimum from 774 nm to ~775 nm can be observed in the following time period of the experiment (7–37 min). The initial delay in plasmonic shift (from 7 to 11 min) can be attributed to the time it takes for the solution to reach the sensor surface. After reaching equilibrium, i.e., no further detectable changes in the position of the reflectance minimum, PBS was passed over the sensor, causing a small shift towards a smaller wavelength of the minimum position. In order to remove the IgG from rabbit antibody from the sensor surface, an abrupt change in pH was made by introducing a 0.1 M acetic acid solution. A further blue shift of the reflectance minimum can be noticed in the corresponding time frame (47–57 min). Finally, PBS was pumped through the flow cell in order to successfully re-establish the baseline. In the next step, a solution of 40 μg mL^{-1} IgG from goat in PBS was injected. The binding affinity of Protein A towards IgG from goat is lower in comparison to IgG from rabbit (Kuo and Lauffenburger, 1993). Consequently, a significantly smaller red shift of the reflectance minimum was detected for IgG from goat (time 67–97 min). The reliability and reusability of the fabricated sensor is demonstrated in Fig. S3 and S4.

3.5. Binding constant of Protein A and IgG from rabbit

The most important and fundamental properties in the study of biochemical and biomedical systems are molecular interactions (Menezes et al., 2012). In order to evaluate the capability of the developed fiber optic plasmonic sensor for biosensing, a concentration dependent study of binding IgG from rabbit to Protein A was performed (Fig. S3). From the position of the reflectance minimum at equilibrium for different IgG concentrations the equilibrium binding constant can be determined by applying a Langmuir fit to the wavelength shift (Fig. 6). Reflectance minimum values of 2–3 trials were averaged and an equilibrium dissociation constant of K_D = (6.71 ± 1.16) 10^{-8} mol L^{-1} for IgG from rabbit to protein A was obtained. This value is in accordance with published values (Pacholski et al., 2006; Saha et al., 2003). The stability of the developed optical fiber plasmonic sensor and the high reproducibility of the obtained sensorgrams are shown in Fig. S3 and Fig. S4 in the Supporting information.

4. Conclusion

To summarize, a method to prepare periodic hole arrays in gold films on optical fiber tips was developed, which is solely based on chemical wet lab techniques. The presented bottom-up approach mainly relies on self-assembly of hydrogel microspheres and transfer of a resulting, perforated gold film on an optical fiber tip. The fiber optic plasmonic sensors and the periodic hole arrays in gold films on flat glass substrates possess a similar bulk sensitivity of ~ 420 nm/RIU. Hence, the transfer step does not affect the sensitivity of the sensors. The label-free biological sensing capabilities of the developed fiber optic plasmonic sensor were demonstrated by monitoring Protein A/IgG interactions in real-time. The measured equilibrium binding constant of Protein A and IgG from rabbit is in good agreement with values reported in literature. The process is very simple and has the potential for large-scale production. The cost-effective fabrication, the high sensitivity, and the very stable as well as

reproducible use in immunoassays make the developed fiber optic plasmonic sensors a versatile platform in the field of biosensors.

Acknowledgement

This work was supported by the German Federal Ministry of Education and Research (BMBF, Grant 03Z22AN12). C.P. gratefully acknowledges funding by the German Research Foundation (DFG, Project no. 286735196).

Declaration of interests

None.

Appendix A. Supplementary material

Supplementary data associated with this article can be found in the online version at doi:10.1016/j.bios.2019.03.020.

References

Boujday, S., Bantegnie, A., Briand, E., Marnet, P.-G., Salmain, M., Pradier, C.-M., 2008. J. Phys. Chem. B 112, 6708–6715.
Cetin, A.E., Etezadi, D., Galarreta, B.C., Busson, M.P., Eksioglu, Y., Altug, H., 2015. ACS Photonics 2, 1167–1174.
Consales, M., Ricciardi, A., Crescitelli, A., Esposito, E., Cutolo, A., Cusano, A., 2012. ACS Nano 6, 3163–3170.
Dhawan, A., Muth, J.F., 2008. Mater. Sci. Eng. B 149, 237–241.
Dhawan, A., Gerhold, M.D., Muth, J.F., 2008. IEEE Sens. J. 8, 942–950.
Ekşioğlu, Y., Cetin, A.E., Petráček, J., 2016. Plasmonics 11, 851–856.
Florinskaya, A., Ershov, P., Mezentsev, Y., Kaluzhskiy, L., Yablokov, E., Medvedev, A., Ivanov, A., 2018. Sensors 18, 1616.
Guan, F., Chen, M., Yang, W., Wang, J., Yong, S., Xue, Q., 2005. Appl. Surf. Sci. 240, 24–27.
Jia, P., Yang, J., 2014. Nanoscale 6, 8836.
Jia, P., Yang, Z., Yang, J., Ebendorff-Heidepriem, H., 2016. ACS Sens. 1, 1078–1083.
Jian, A., Deng, L., Sang, S., Duan, Q., Zhang, X., Zhang, W., 2014. IEEE Sens. J. 14, 3229–3235.
Klantsataya, E., Jia, P., Ebendorff-Heideprim, H., Monro, T.M., Francois, A., 2017. Sensors 17, 12.
Kuo, S.C., Lauffenburger, D.A., 1993. Biophys. J. 65, 2191–2200.
Lan, X., Cheng, B., Yang, Q., Huang, J., Wang, H., Ma, Y., Shi, H., Xiao, H., 2014. Sens. Actuators B-Chem. 193, 95–99.
Lin, Y., Zou, Y., Lindquist, R.G., 2011. Biomed. Opt. Express 2, 478.
Lipomi, D.J., Martinez, R.V., Kats, M.A., Kang, S.H., Kim, P., Aizenberg, J., Capasso, F., Whitesides, G.M., 2011. Nano Lett. 11, 632–636.
Liu, Z., Liu, L., Zhu, Z., Zhang, Y., Wei, Y., Zhang, Y., Yang, J., Yuan, L., 2017. Opt. Commun. 403, 290–295.
Mayer, K.M., Hafner, J.H., 2011. Chem. Rev. 111, 3828–3857.
McMahon, J.M., Henzie, J., Odom, T.W., Schatz, G.C., Gray, S.K., 2007. Opt. Express 15, 18119.
Menezes, J.W., Barea, L.A.M., Chillcce, E.F., Frateschi, N., Cescato, L., 2012. IEEE Photonics J. 4, 544–551.
Najiminaini, M., Vasefi, F., Kaminska, B., Carson, J.J.L., 2011. Opt. Express 19, 26186.
Pacholski, C., Yu, C., Miskelly, G.M., Godin, D., Sailor, M.J., 2006. J. Am. Chem. Soc. 128, 4250–4252.
Piliarik, M., Vaisocherová, H., Homola, J., 2009. In: Rasooly, A., Herold, K.E. (Eds.), Biosensors and Biodetection. Humana Press, Totowa, NJ, pp. 65–88.
Pisco, M., Galeotti, F., Quero, G., Grisci, G., Micco, A., Mercaldo, L.V., Veneri, P.D., Cutolo, A., Cusano, A., 2017. Light Sci. Appl. 6, 16229.
Pumera, M., 2011. Mater. Today 14, 308–315.
Quint, S.B., Pacholski, C., 2009. J. Mater. Chem. 19, 5906–5908.
Quint, S.B., Pacholski, C., 2011. Soft Matter 7, 3735–3738.
Quint, S.B., Pacholski, C., 2014. J. Mater. Chem. C 2, 7632–7638.
Rengarajan, R., Mittleman, D., Rich, C., Colvin, V., 2005. Phys. Rev. E 71.
Riccardi, A., Crescitelli, A., Vaiano, P., Quero, G., Consales, M., Pisco, M., Esposito, E., Cusano, A., 2015. Analyst 140, 8068–8079.
Saha, K., Bender, F., Gizeli, E., 2003. Anal. Chem. 75, 835–842.
Sahoo, P.R., Swain, P., Nayak, S.M., Bag, S., Mishra, S.R., 2016. Vet. World 9, 1338–1342.
Saito, M., Uchida, N., Furutani, S., Murahashi, M., Espulgar, W., Nagatani, N., Nagai, H., Inoue, Y., Ikeuchi, T., Kondo, S., et al., 2018. Microsyst. Nanoeng. 4, 17083.
Siegfried, T., Ekinci, Y., Martin, O.J.F., Sigg, H., 2013. ACS Nano 7, 2751–2757.
Smythe, E.J., Dickey, M.D., Whitesides, G.M., Capasso, F., 2009. ACS Nano 3, 59–65.
Sumner, C., Sabot, A., Turner, K., Krause, S., 2000. Anal. Chem. 72, 5225–5232.
Thio, T., Ghaemi, H.F., Lezec, H.J., Wolff, P.A., Ebbesen, T.W., 1999. J. Opt. Soc. Am. B 16, 1743.
Turkevich, J., Stevenson, P.C., Hillier, J., 1951. Discuss. Faraday Soc. 11, 55–75.
Ullrich, S., Scheeler, S.P., Pacholski, C., Spatz, J.P., Kudera, S., 2013. Part. Part. Syst. Charact. 30, 102–108.
Wang, H., Wang, X., Wang, J., Fu, W., Yao, C., 2016. Sci. Rep. 6.
Weiler, M., Quint, S.B., Klenk, S., Pacholski, C., 2014. Chem. Commun. 50, 15419–15422.
Wijaya, E., Lenaerts, C., Maricot, S., Hastanin, J., Habraken, S., Vilcot, J.-P., Boukherroub, R., Szunerits, S., 2011. Curr. Opin. Solid State Mater. Sci. 15, 208–224.
Yonzon, C.R., Jeoung, E., Zou, S., Schatz, G.C., Mrksich, M., Van Duyne, R.P., 2004. J. Am. Chem. Soc. 126, 12669–12676.